Application of EMR Signature in Health Assessment and Monitoring of IGBT-Based Converters

Rajashree Biswas and Aurobinda Routray, *Member, IEEE*

***Abstract*—In this paper, a non-invasive method based on electromagnetic radiation (EMR) signature is proposed for the health assessment of the converters. Converters use insulated gate bipolar transistor (IGBT) because of its robustness. However, it suffers from internal degradation due to the rapid power cycle and thermal stress. Degradation of IGBT primarily increases the turn-OFF time as a consequence of elevated junction temperature. The coupling of IGBT with the parasitics of the circuit results in EMR and depends on the turn-OFF time of IGBT. It has been found that the EMR signature reduces with the increase in turn-OFF time. This concept is taken forward for the health assessment of the converters. However, in a practical scenario, the EMR generated from multiple converters get mixed up. This is commonly known as a problem of near-field source localization. We use a uniform linear array to capture the EMR signals near the converters. Subsequently, ESPRIT and MUSIC algorithms are used to localize all the converters. An inverse transformation of the localization algorithm separates the EMR signature of all the individual converters. The proposed health assessment algorithm computes the degradation level of converters, and the experimental results validate the proposed approach.**

***Index Terms*—Electromagnetic radiation (EMR), estimation of signal parameters via rotation invariance techniques (ESPRIT), fault-diagnosis, health-assesment, multiple signal classification (MUSIC), uniform linear array (ULA).**

I. Introduction

HIGH-FREQUENCY converters prevalently make use of insulated gate bipolar transistor (IGBT) for its high current and voltage rating, and short circuit withstands capability up to 10 μs. In spite of all these features, about 38% to 40% of total faults in power converters occur due to the failure of the power devices [1]. The gradual degradation of the IGBT not only deteriorates the converter performance but also affects the downstream devices. Health assessment and monitoring can timely detect these degradations and faults. The health assessment is a continuous process which compares the operating characteristic of the system with the standard characteristic and finds out the significant differences which may be an indicator of degradation or failure. It saves the whole system from serious deterioration or sudden breakdown.

Manuscript received November 28, 2018; revised February 12, 2019 and April 4, 2019; accepted May 3, 2019. Date of publication May 12, 2019; date of current version November 12, 2019. Recommended for publication by Associate Editor A. Lindemann. *(Corresponding author: Rajashree Biswas.)*

The authors are with the Department of Electrical Engineering, Indian Institute of Technology Kharagpur, Kharagpur 721302, India (e-mail: rajashreeee20@gmail.com; aurobinda.routray@gmail.com).

Color versions of one or more of the figures in this paper are available online at http://ieeexplore.ieee.org.

Digital Object Identifier 10.1109/TPEL.2019.2916358

High-frequency and high-power operation of the converters make the power device go through extreme power cycles, environmental stresses, and overloading conditions [1]. This leads to the degradation of power devices. The degradation can be found out by measuring the aging precursors [2], [3]. Different approaches have been used over the past several years for the health-monitoring of the converters. In [4], [5], monitoring of power devices of the converter is done by measuring saturation-region resistance, and online V_{ce} respectively. An online health monitoring and aging detection process have been presented in [6], [7], respectively. It has been seen that various parameters of IGBT, such as leakage current, gate threshold voltage, ON-state voltage, turn-OFF time, and the junction temperature change with the age of the device [8], [9]. Among these parameters threshold voltage, junction temperature, and turn-OFF time have a linear relation with the device aging. Also, the turn-OFF time shows a remarkable change in comparison to the gate threshold voltage and ON-state voltage. The junction temperature and the turn-OFF time are mutually dependent on each other. However, the turn-OFF time is considered as monitoring parameter as it indicates the pre-latching condition [10], switching power loss [11], and has a direct impact on the electromagnetic radiation (EMR) generated by the device.

The aforementioned methods are based on the various in-circuit measurement of the converter. In [12], the proposed method does not require additional hardware but depends on the available measurements. The practical implementation of these methods requires complex measurement, cost-effective sensors, and a skilled workforce to monitor. Apart from this, these methods are limited to the monitoring of a single converter. The EMR signature method overcomes these limitations and provides a non-invasive way of health assessment.

Over the past few decades, EMR has been successfully used in fault diagnosis of permanent magnet synchronous machines [13], asynchronous machines [14], condition monitoring of power components in electric grid [15], and locating faults in electrical cables [16]. Authors of [17] have been studied various types of faults of the converter connected to a grid using the EMR of the converter. However, there are no deep-dive studies based on the relationship between the degradation level of the devices, and the EMR signature is present in the literature. In [18], we have shown that the EMR signatures are related to the various aging parameters of the IGBT, and can be used for health assessment of single IGBT-based converters. However, the method fails when multiple converters operate simultaneously. The converters are the source of EMR, and simultaneous

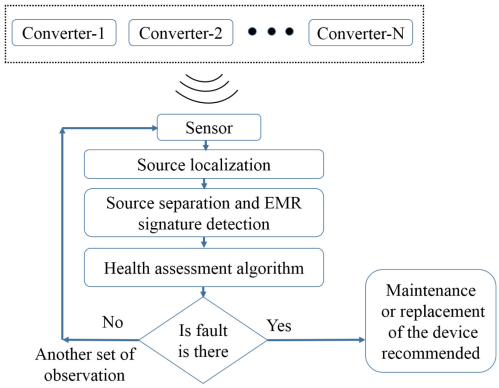

Fig. 1. Proposed health-assesment algorithm layout.

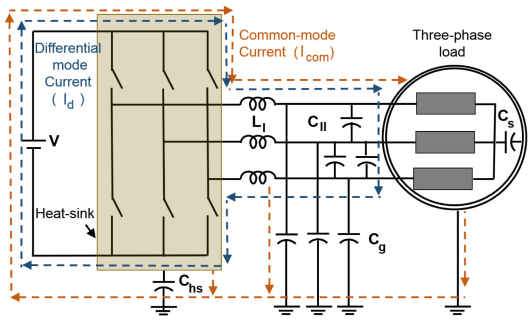

Fig. 2. Common mode and differential mode currents of converter.

operation of converters render into a localization problem. As the EMR is available in the Fresnel region only, it gives rise to near-field source localization problem.

In this paper, we are proposing a method for continuous health assessment of multiple converters by way of EMR signature analysis. This has been done by investigating on turn-OFF characteristic of the IGBT through EMR signatures. In multiple converter setups, the EMR generated from various converter gets mixed up. Here the issue is to detect these abnormal signatures and separate them for health assessment of converters. Several methods, such as 2D MUSIC [19], 2D ESPRIT [20], combination of MUSIC with ESPRIT [21], and blind source separation (BSS) [22], etc. have been used to find out the direction of arrival (DOA) and the distance of the converter. Here, we are using the combination of ESPRIT and MUSIC algorithm due to its high resolution and low computational complexity in comparison to BSS and 2D methods. Therefore the proposed method works on the principals of localization, separation, and detection as mentioned in Fig. 1.

The proposed methodology contributes to the field of health assessment of converters in the following ways.

1) Establishing the relation between IGBT turn-OFF time with the EMR signature.
2) Incorporating source localization method to compute the degradation level of multiple converters simultaneously.
3) Introducing a threshold based health assessment algorithm to determines the degradation level of the converter.

The main advantage of the proposed method is that any existing converter can also adopt this method of health assessment as it is non-invasive, does not need any in-circuit interventions, and the user does not need to have a deep knowledge of the power electronics to check the converter health condition.

II. EMR Signature Method

The fast switching of power devices generates unwanted voltage and currents coupled with the parasitic elements of the circuit [23]. Based on the paths of coupling the high-frequency current, it is categorized as common-mode (I_{com}) and differential mode (I_d) current. The differential mode current is due to coupling of transient line-to-line voltage with stray inductances (L_l) and line-to-line capacitance(C_{ll}) (as shown in Fig. 2). The fast $\frac{dv}{dt}$ of common-mode voltage excites the parasitic heat-sink capacitor (C_{hs}), load heat-sink capacitance (C_s) and ground capacitance (C_g), which results in the common-mode current. The loops of common-mode currents are larger than the differential-mode currents (as shown in Fig. 2), which act as an antenna for EMR [24].

A. Physics of IGBT During Turn-Off

The physics of the IGBT says that during turn-OFF, the carrier concentration across the drift region determines the turn-OFF time of the device [25]. Due to electrical and thermal stress, the operating junction temperture of the device gradually increases [8] and the electron–hole recombination rate decreases [26]. The concentration of intrinsic carriers (n_i in cm^{-3}) and total electrons in the conduction band (n in cm^{-3}) can be expressed as follows [27], [28]:

$$n_i = \sqrt{N_c N_v} e^{\frac{-E_G}{2kT}} \quad n = n_i e^{\frac{E_F - E_G}{kT}} \tag{1}$$

where N_C and N_V are the effective electron and hole density (cm^{-3}) respectively. E_F and E_G are energy at Fermi level and conduction band respectively. k is the Boltzmann constant (8.62×10^{-5}eV/K), and T is the temperature (in Kelvin). The exponential temperature dependence of n_i dominates the much smaller temperature dependency in (1) than other terms. Hence, with the increase in thermal stress, the junction temperature of the device will increase, which further elevate the concentration of free carriers. High carrier concentration eventually increases the turn-OFF time.

B. Converter as a Hertzian Dipole

During the switching operation, the power device module behaves as the pair of charges with inverse polarity connected by a conductor as shown in Fig. 3 [29]. This pair of charges considered as a Hertzian dipole. The near field is divided into two regions, such as active and radiative (otherwise known as the Fresnel region). The active region is very close to the source and finding the relation between the different parameters of the field is difficult. In the radiation field region, the electric and magnetic fields are orthogonal to each other. Therefore the field parameters are predictable. This region is suitable for our measurement and the distance between point P, and the dipole is far

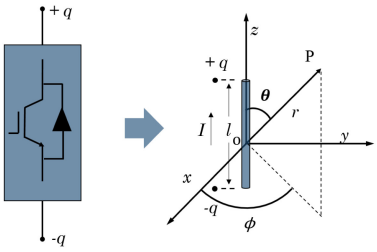

Fig. 3. Radiated electromagnetic field by a current element.

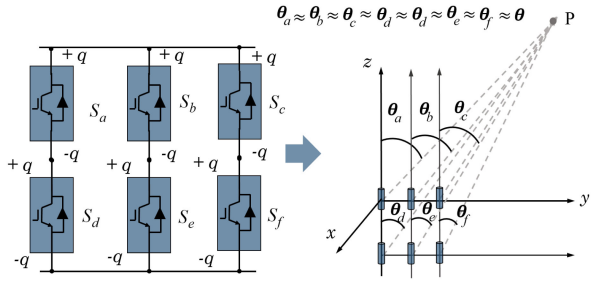

Fig. 4. Converter operating as a combination of multiple Hertzian dipole.

greater than the radiation wavelength. The general expression for the radiated electric and magnetic field in the radiative region is given by (2) and (3), respectively, where E and H are the electric and magnetic fields at the point P, respectively. I and l are the current passing through and length of the dipole respectively. $\beta = \omega\sqrt{\mu\epsilon}$ is the wave number, where μ is the permittivity, and ϵ is the permeability of the medium. $\overrightarrow{a_r}$ and $\overrightarrow{a_\theta}$ are unit vectors of radial and angle direction at point P.

$$E = \frac{\eta I l}{2\pi r^2}\left(1+\frac{1}{j\beta r}\right)\cos\theta e^{-j\beta r}\overrightarrow{a_r} + \frac{jIl\eta\beta}{4\pi r}\left(1+\frac{1}{j\beta r}-\frac{1}{\beta^2 r^2}\right)\sin\theta e^{-j\beta r}\overrightarrow{a_\theta} \quad (2)$$

$$H = \frac{j\beta I l}{4\pi r}\left(1+\frac{1}{j\beta r}\right)\sin\theta e^{-j\beta r}\overrightarrow{a_\phi}. \quad (3)$$

It is apparent from (2) and (3) that the electric and magnetic fields depend upon the current and contain the information about distance ($\overrightarrow{a_r}$) and DOA ($\overrightarrow{a_\theta}$). Here I is the cause of radiation, and for this case, it is the common-mode current of the converter. The common-mode current of a converter can be expressed as

$$I = (C_{hs} + C_g + C_s) \times \frac{dV}{dt} \quad (4)$$

where $\frac{dV}{dt}$ is the rate of change of the voltage across the power device, this change in dV is constant for a voltage source inverter. However, dt is the rate at which the power device is turning ON or OFF. Hence the common-mode current only depends on the switching time of the IGBT.

Power converters are sources of EMR, and a ULA is used to capture this radiation. The power spectrum of this captured magnetic field is denoted as the EMR spectrum, and the peak of the spectrum is presented as the EMR signature. The EMR signature of a converter can be expressed as follows:

$$\text{EMR Signature} = \text{peak of}\left(10\log_{10}\left[\frac{1}{F_s N}\left\|X(e^{j\omega})\right\|^2\right]\right). \quad (5)$$

where F_s and N are sampling frequency and length of the time domain signal respectively. $X(e^{j\omega})$ is the fast Fourier transform of the electromagnetic field captured by the ULA. Due to the rapid power cycle the turn-OFF time of the IGBT increases (As explained in II-A). It is apparent from (4) that with the increase in turn-OFF time, the common-mode current magnitude will reduce. This will result in a reduction in EMR signature, as it depends upon the EMR caused by common-mode current.

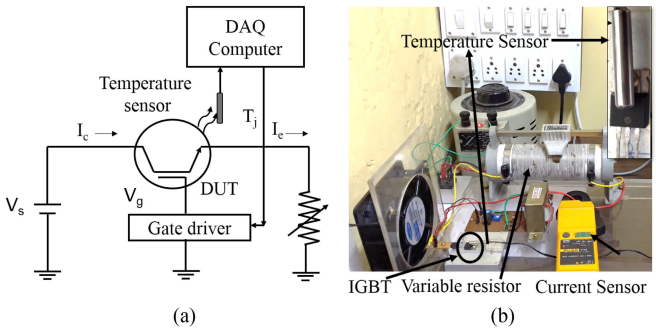

Fig. 5. (a) Schematic, (b) experimental setup of the power cycle test.

In a converter, more than one IGBTs are present as shown in Fig. 4. The IGBTs are compactly packed inside the converter such that the radiation of all individual Hertzian dipole at point P is inseparable. The age of the IGBT is increased by accelerated power cycling methods. Since all the IGBTs in a converter, go through the same number of the power cycles, they radiate in the same frequency range. At a particular time, the EMR signature of a power converter is the aggregated effect of the EMR signature of each IGBT. The reduction of EMR signature denotes the increase in turn-OFF time. This signifies the increase in junction temperature, which increases leakage current [9]. Hence the EMR signature is related to all degradation parameter, and gradual fall of EMR signature indicates poor health of the IGBT and the converter as well.

C. Power Cycle Test Result

The gradual degradation to IGBT is induced by a constant current power cycling method [30]. The schematic and experimental setup of the power cycling method is shown in Fig. 5. In this procedure, the power devices are loaded 1.5 times of the rated value. The part name of the device under test is STGF6NC60HD. Each power cycle consists of 0.3 s ON and 0.7 s OFF time. The temperature (T_j) of the device is raised by the conduction losses and observed around 200 °C. The IGBTs are subjected to a power cycling test for 30 minutes followed by a sufficient cooling time. The IGBTs are then operated at rated current and a frequency of 10 KHz. The parameters (leakage current, turn-OFF time, operating junction temperature, and ON-state voltage) were measured

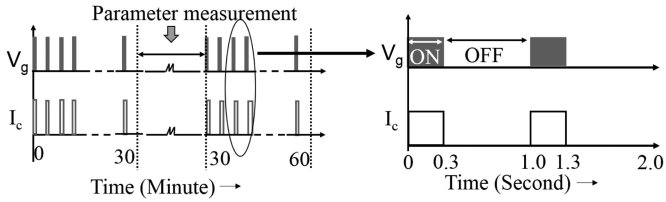

Fig. 6. Power cycle timing diagram.

TABLE I
IGBT1 PARAMETERS AT DIFFERENT POWER CYCLE LEVEL

Power cycling Time(Minute)	Leakage current (mA)	Turn-off Time(μs)	on-state Voltage(V)	Junction Temperature(^{0}C)	EMR Signature(dB)
0	0.1	2.9	1.0	30	-80
30	5	5	0.9	42	-91
60	15	7.1	0.5	53	-102
90	38	10.5	1.6	68	-120

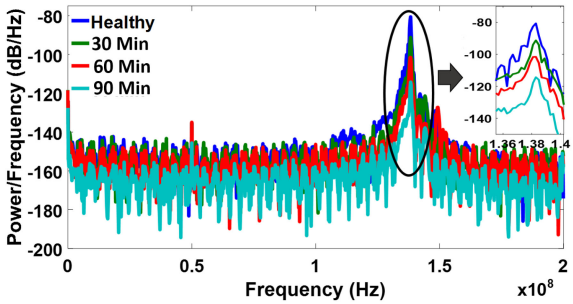

Fig. 7. EMR signature of IGBT1 at different power cycle level.

TABLE II
VARIATION OF EMR SIGNATURE AT DIFFERENT POWER CYCLE LEVEL

IGBT Number	EMR Signature (dB)			
	0 min	30 min	60 min	90 min
IGBT1	-80	-91	-102	-120
IGBT2	-78	-88	-100	-118
IGBT3	-83	-93	-103	-119
IGBT4	-83	-94	-103	-118
IGBT5	-79	-89	-98	-116
IGBT6	-77	-89	-99	-118
IGBT7	-82	-91	-100	-120
IGBT8	-80	-92	-103	-121
IGBT9	-81	-91	-101	-119
IGBT10	-79	-90	-99	-118

at the rated operating condition. Then the IGBTs are subjected to another 30 min of power cycling test as shown Fig. 6. This overstress method is repeated until the power device under test fails to operate.

The effect of the power cycle test on an IGBT is shown in Table I and the corresponding EMR signature is shown in Fig. 7. It is observed from the Table I that with the power cycling time the junction temperature increases. The raised junction temperature results in an increase in turn-OFF time and leakage current. The EMR signature gradually reduces with these parameters which validate the relationship we have established in Sections II-A and II-B. The variation of EMR signatures of ten IGBTS is shown in Table II.

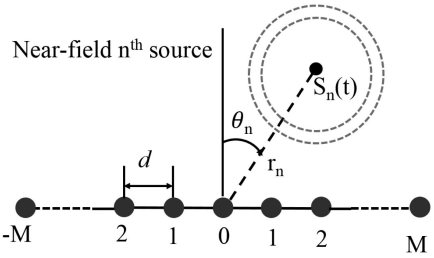

Fig. 8. Array signal model.

III. CONVERTER LOCALIZATION

The complete health-monitoring layout consists of five main segments as shown in Fig. 1. In this section, the localization of converters is explained. For which the assumptions made in this paper are 1) the EMR signals generated by each converter are independent of other peripheral EMR sources; 2) the noise capture through ULA is Gaussian noise and assumed to be independent of the source signal; and 3) the number of sensors must be greater than the number of sources.

A single loop antenna was used to capture the EMR of a single IGBT-based converter, which was considered to be enough for the analysis in [18]. However, in the case of multiple converters, the number of sensors has to be increased to detect individual sources. For the N number of converter localization, it demands $2M+1$ number of sensors [21] such that $(2M+1) >= (2N+1)$. A uniform linear array (ULA) of loop antennas is used to captures the near-field EMR, and the model is shown in Fig. 8. Here, d is the distance between the receiving sensors. The received signals (i.e., $x(k)$) of mth sensor (i.e., loop antenna) from nth sources (i.e., converter) at kth instant is represented as

$$x_m(k) = \sum_{n=1}^{N} s_n(k) e^{j\tau_{mn}} + w_m(k)$$
$$-M \leq m \leq M \quad \text{and} \quad k = 1, 2, 3, ...K \tag{6}$$

where s_n, θ_n, and r_n denotes the nth source, the angle of arrival of the nth source, and distance of nth source from the $zero$th sensor respectively. τ_{mn} is the time delay to receive the signal from nth source to mth sensor with reference to $zero$th sensor which is given as

$$\tau_{mn} = \frac{2\pi}{\lambda}\left(\sqrt{r_n^2 + (md)^2 - 2r_n md\sin(\theta_n)} - r_n\right). \tag{7}$$

The second-order taylor expansion is given as

$$\tau_{mn} = m\omega_n + m^2\phi_n$$
$$l\omega_n = -2\pi\frac{d}{\lambda}\sin(\theta_n)$$
$$\phi_n = \pi\frac{d^2}{\lambda r_n}\cos^2(\theta_n). \tag{8}$$

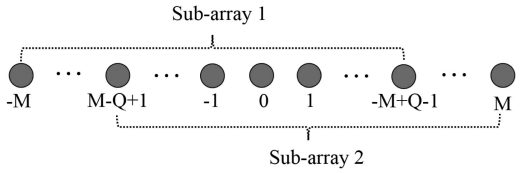

Fig. 9. Subarray model for implementing ESPRIT.

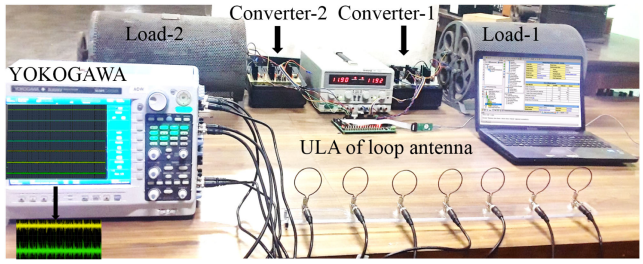

Fig. 10. Experimental setup of two experiments.

Equation (6) can be written as following matrix form for L number of sample data

$$x(k) = As(k) + w(k) \tag{9}$$

where $x(k)=[x_M(k),\ldots,x_0(k),\ldots,x_{-M}(k)] \in C^{(2M+1)\times L}$ is capatured electomagnetic radiation, $s(k)=[s_1(k),\ldots,s_N(k)] \in C^{N\times L}$ is source signal, $w(k)=[w_{-M}(k),\ldots,w_M(k)] \in C^{2M+1\times L}$ is additive Gaussian noise and $A=[a(\omega_1,\phi_1)\ a(\omega_2,\phi_2)\ldots a(\omega_N,\phi_N)] \in C^{(2M+1)\times N}$ steering vector whose elements are given by (10).

$$a(\omega_n,\phi_n) = \begin{bmatrix} e^{-j\omega_n M+j\phi_n M^2} \\ \vdots \\ 1 \\ \vdots \\ e^{j\omega_n M+j\phi_n M^2} \end{bmatrix} \tag{10}$$

The covariance matrix of received signal is given in equation.

$$R_x = E\left[x(k)\,x^H(k)\right] = AR_SA^H + \sigma^2 I. \tag{11}$$

H denotes the conjugate transpose of the matrix, σ^2 power of noise and $R_S = E[s(k)s^H(k)]$ is the signal covariance matrix.

A. DOA Estimation Using ESPRIT

In this paper high-resolution subspace-based method ESPRIT is used to find out the DOA of the EMR sources. It is based upon the rotational invariance property of the signal subspace [31]. The ULA is divided into two subarray to apply the ESPRIT method as shown in Fig. 9. The first subarray is formed by considering the first Q elements and the second subarray is formed by considering the last Q elements. Let A_1 be the steering matrix of subarray1, and A_2 be the steering matrix of subarray2. Both the matrixes are related in (12) due to the symmetry of the array structure

$$\begin{aligned} A_1 &= [a_1(\omega_1,\phi_1)\cdots a_1(\omega_N,\phi_N)] \\ A_2 &= [a_2(\omega_1,\phi_1)\cdots a_2(\omega_N,\phi_N)] \\ A_2 &= [\Phi(\omega_1)a_1(\omega_1,\phi_1)\cdots\Phi(\omega_N)a_1(\omega_N,\phi_N)] \end{aligned} \tag{12}$$

where Φ is a diagonal matrix as follows:

$$\Phi(\omega_n) = \begin{bmatrix} e^{j2\omega_n M} & & 0 \\ & \ddots & \\ 0 & & e^{j2\omega_n(M-Q+1)} \end{bmatrix}. \tag{13}$$

For implementing ESPRIT, the sources eigenvectors are further divided into two subparts U_s^1 and U_s^2. $U_s^1$and U_s^2 denote the first and last Q rows of U_s, respectively. Due to this, we can write $U_s^1 = A_1G$, and $U_s^1 = JA_2G$, where G is a full rank matrix of rank Q and J is a unit counter diagonal matrix. The DOA $(\hat{\omega}_n)$ is found from the nulls of the following spectrum, where $E=[JU_s^2 - \Phi(\omega_n)U_s^1]$

$$P_{GE}(\omega_n) = \det[E^HE]. \tag{14}$$

B. Range Estimation Using MUSIC

The covariance matrix obtained from ULA is always Hermitian, and the eigenvectors of this type of matrix are orthogonal to each other. MUSIC algorithm is based upon this basic idea of orthogonality of noise to signal sub-space [32]. Here subspace means the eigenvectors of either noise or sources. The peak of the spectrum function, constituted by these two orthogonal spectra is our desired result. The DOA θ_n is determined by ESPRIT. Substituting this value in the steering matrix (10), the order of the localization problem reduces. Now, the MUSIC algorithm can be used to find out the distance of the converters. The range of the converter is estimated by the peaks of the following spectrum:

$$\begin{aligned} P_M(\phi_n) &= \frac{1}{a^H(\omega_n,\phi_n)U_nU_n^Ha(\omega_n,\phi_n)}, n=1,2,\ldots,N \\ \hat{r}_n &= \arg\max[P_M(\phi_n)]. \end{aligned} \tag{15}$$

IV. Source Localization Experiment

Two experiments have been carried out to test the performance of ESPRIT and MUSIC. The experimental setup for such an experiment is shown in Fig. 10. The experiments are carried out in a laboratory environment where there are no other dominant EMR sources present. Detail parameters of the experiment, such as the distance of the sources from the array, separation between the converters are shown in Fig. 11. The converter-1 and converter-2 are three-phase converters with rating 1 KVA and 600 VA, respectively. The converter-1 is built with the IGBTs power cycled up to 40 min. Similarly, the converter-2 is built with IGBTs power cycled up to 20 min. Seven sensors are used in ULA for both the experiments. The sensors are loop antennas which are used as a receiver due to its wide frequency range and high efficiency. The loop antennas are made as per IEC 61967-3 Standard. The details of the design are provided in Fig. 12. The maximum radiations of converters are observed around 600 MHz, signal wavelength $\lambda = 0.50$ m, and the inter-element spacing is $d = 0.10$ m$(d <= \lambda/4)$.

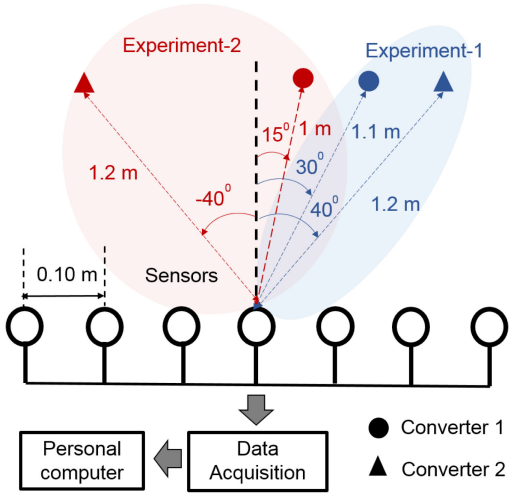

Fig. 11. Experimental layout of two experiments.

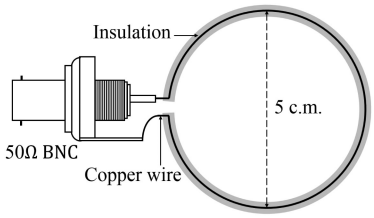

Fig. 12. Design details of loop antenna.

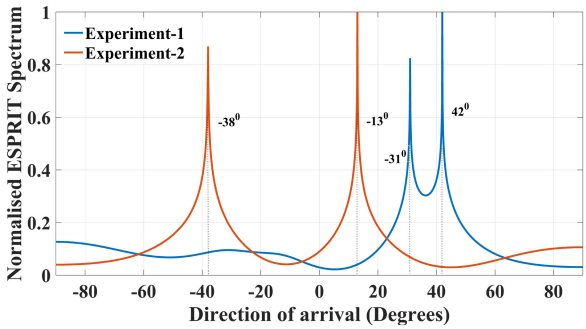

Fig. 13. ESPRIT spectrum showing the DOA of converters in experiment-1 and experiment-2.

The signals captured in ULA are then analyzed using the classical algorithms. ESPRIT determines the DOA of the two converters, and MUSIC estimates the distance of the converters from $zero$th sensor. Figs. 13 and 14 show such results and the percentage of error is listed in Table III. Once both the parameters of the steering matrix are determined, the separated source signals can be obtained from (9).

V. Health Assessment Algorithm

The degradation of the power device in a converter is a gradual process and may take over months and years. Therefore, the proposed health assessment algorithm continuously compares the EMR signatures with two threshold bands and determines the degradation level of the converter. The first band consists of

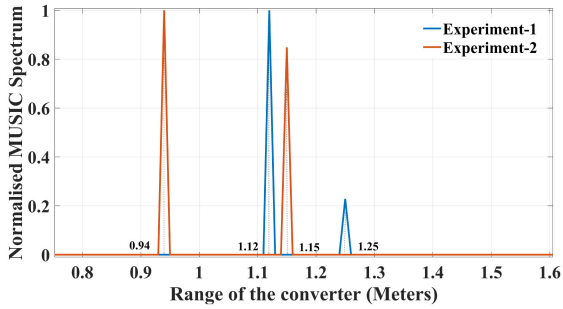

Fig. 14. MUSIC spectrum showing the range of converters in experiment-1 and experiment-2.

TABLE III
Percentage of Error of the DOA Experiment

	DOA			Range		
Experiment-1	Real value	Observed value	Error	Real value	Observed value	Error
Converter-1	30^0	31^0	3.33%	1.1 m	1.12 m	2%
Converter-2	40^0	42^0	5%	1.2 m	1.25 m	5%
	DOA			**Range**		
Experiment-2	Real value	Observed value	Error	Real value	Observed value	Error
Converter-1	15^0	13^0	13.33%	1.0 m	0.94 m	6%
Converter-2	-40^0	-38^0	5%	1.2 m	1.15 m	5%

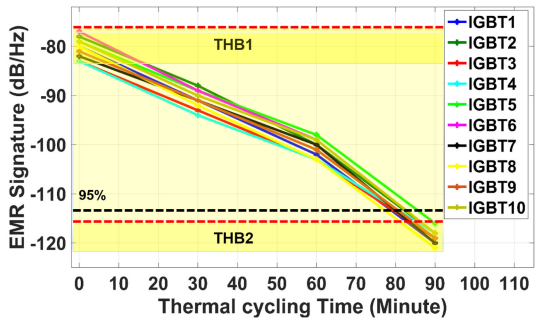

Fig. 15. Health assessment algorithm.

the EMR signatures of IGBTs at the healthy condition, denoted as threshold band-1 (THB-1). The second band consists of EMR signature values prior to failure, denoted as threshold band-2 (THB-2). The data of Table II is plotted, and the two threshold bands are shown in Fig. 15.

Fig. 16 shows the proposed algorithm. The first step is to take a dataset of 1000 samples from the ULA. In the next step, ESPRIT and MUSIC are used to determine the location of the converters (i.e., θ_n and r_n). Substituting the localization parameter in the steering vector of (9), $s(t)$ is estimated assuming the noise is independent of the source signal. Now, the peak of the separated signal spectrum is the EMR signature (EMRS). THB is the threshold band which specifies the timeline to show the health condition of the converter. DGL and PGDL denote the degradation level and the percentage of degradation level respectively. The formulations of these variables are shown in Fig. 16. We can see from the graph (Fig. 15) that the slope of the EMR signature increases as the power cycling time increases. The slope is highest between the cycling time of 60–90 min. The case where the degradation level of converters is more than or equal

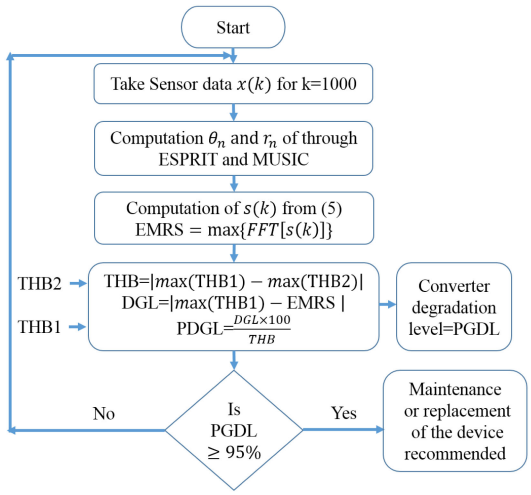

Fig. 16. Health assessment algorithm.

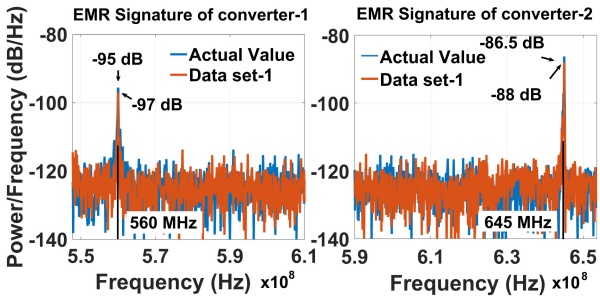

Fig. 17. Separated EMR signatures of two converters.

to 95%, i.e., as soon as it about to enter into THB-2, it demands special attention. It indicates a condition, where more than one power devices are operating in a pre-latching condition. At this point, the replacement of the existing device will save the whole system from sudden failure. The health assessment algorithm localizes and separates the EMR signatures of converter-1 and converter-2 of experiment-1 (Fig. 17). The degradation level of converter-1 and converter-2 are detected to be 51% and 23%, respectively.

The accuracy of the proposed algorithm is computed by repeating experiment-1 and experiment-2. But, this time instead of the simultaneous operation of two converters, one converter is operated at the same time keeping the other in the OFF condition. The individual EMR signature of both the converters is computed by (5). The converter localization step is omitted to eliminate the errors due to the localization parameter. The EMR signatures obtained from this experiment are denoted as "actual value". The actual values of both the converters are measured for experiment-1 and experiment-2. Then different data sets are collected from the previously done experiments (Section IV), where two converters are operated simultaneously. In this case, the EMR signatures of the converters are computed by the proposed health assessment algorithm. It is to be noted that the data sets are different runs of the same experiment, at similar ambient conditions. The percentage of error is calculated by comparing the "actual value" with the EMR signatures obtained from different datasets and listed in Table IV.

TABLE IV
PERCENTAGE OF ERROR OF THE EMR SIGNATURE METHOD

Converter Number			Converter-1	Converter-2
EMR signature (dB/Hz)	Experiment-1	**Actual value**	**-95**	**-86.5**
		Data set-1	-97	-88
		Error	2.1%	1.7%
		Data set-2	-97	-88.5
		Error	2.1%	2.3%
		Data set-3	-96	-87.5
		Error	1.1%	1.2%
	Experiment-2	**Actual value**	**-94.5**	**-86.5**
		Data set-1	-96	-89
		Error	1.6%	2.9%
		Data set-2	-96	-88.5
		Error	1.6%	2.3%
		Data set-3	-97	-88
		Error	2.6%	1.7%

VI. CONCLUSION

A non-invasive way of health assessment and monitoring of converters through EMR signature has been presented in this paper. Accelerated aging test on IGBT demonstrated that with the increase in the number of power cycles the turn-OFF time, leakage current, and the junction temperature of the device increases. The relationship between the EMR signature and the turn-OFF time of the IGBT has been established. The reduced EMR signature indicates the increase in turn-OFF time as well as the degradation of IGBT. To solve the multiple converter health assessment problem classical methods like ESPRIT and MUSIC has been used to locate and separate the EMR signatures of converters. The source localization experiment results showed the DOA and the range of converters. The health assessment algorithm identified the degradation level of a converter based on its EMR signature analysis. The proposed method can be easily implemented to environments where multiple converters are operating simultaneously without any physical contact with the converter.

REFERENCES

[1] F. W. Fuchs, "Some diagnosis methods for voltage source inverters in variable speed drives with induction machines—A survey," *Ind. Electron. Soc.*, no. 3, pp. 1378–1385, 2003.
[2] H. Oh, B. Han, P. McCluskey, C. Han, and B. D. Youn, "Physics-of-failure, condition monitoring, and prognostics of insulated gate bipolar transistor modules: A review," *IEEE Trans. Power Electron.*, vol. 30, no. 5, pp. 2413–2426, May 2015.
[3] K. B. Pedersen and K. Pedersen, "Dynamic modeling method of electro-thermo-mechanical degradation in IGBT modules," *IEEE Trans. Power Electron.*, vol. 31, no. 2, pp. 975–986, Feb. 2016.
[4] L. Ren, C. Gong, and X. Chen, "Monitoring transistor degradation in power electronic converters using saturation-region resistance," in *Proc. IEEE Energy Convers. Congr. Expo.*, 2017, pp. 1148–1153.
[5] S. Bęczkowski, P. Ghimre, A. R. de Vega, S. Munk-Nielsen, B. Rannestad, and P. Thøgersen, "Online VCE measurement method for wear-out monitoring of high power IGBT modules," in *Proc. 15th Eur. Conf. Power Electron. Appl.*, 2013, pp. 1–7.
[6] J. Morroni, A. Dolgov, M. Shirazi, R. Zane, and D. Maksimovic, "Online health monitoring in digitally controlled power converters," in *Proc. IEEE Power Electron. Spec. Conf.*, 2007, pp. 112–118.
[7] J. K. Mann, S. Perinpanayagam, and I. Jennions, "Aging detection capability for switch-mode power converters," *IEEE Trans. Ind. Electron.*, vol. 63, no. 5, pp. 3216–3227, May 2016.

[8] N. Patil, J. Celaya, D. Das, K. Goebel, and M. Pecht, "Precursor parameter identification for insulated gate bipolar transistor (IGBT) prognostics," *IEEE Trans. Rel.*, vol. 58, no. 2, pp. 271–276, Jun. 2009.
[9] S. Dusmez, S. H. Ali, M. Heydarzadeh, A. S. Kamath, H. Duran, and B. Akin, "Aging precursor identification and lifetime estimation for thermally aged discrete package silicon power switches," *IEEE Trans. Ind. Appl.*, vol. 53, no. 1, pp. 251–260, Jan./Feb. 2017.
[10] D. W. Brown, M. Abbas, A. Ginart, I. N. Ali, P. W. Kalgren, and G. J. Vachtsevanos, "Turn-off time as an early indicator of insulated gate bipolar transistor latch-up," *IEEE Trans. Power Electron.*, vol. 27, no. 2, pp. 479–489, Feb. 2012.
[11] A. Ramamurthy, S. Sawant, and B. Baliga, "Modeling the [dv/dt] of the IGBT during inductive turn off," *IEEE Trans. Power Electron.*, vol. 14, no. 4, pp. 601–606, Jul. 1999.
[12] M. Bhardwaj, S. Choudhury, R. Poley, and B. Akin, "Online frequency response analysis: A powerful plug-in tool for compensation design and health assessment of digitally controlled power converters," *IEEE Trans. Ind. Appl.*, vol. 52, no. 3, pp. 2426–2435, May/Jun. 2016.
[13] Y. Da, X. Shi, and M. Krishnamurthy, "A new approach to fault diagnostics for permanent magnet synchronous machines using electromagnetic signature analysis," *IEEE Trans. Power Electron.*, vol. 28, no. 8, pp. 4104–4112, Aug. 2013.
[14] M. Barzegaran, A. Mazloomzadeh, and O. A. Mohammed, "Fault diagnosis of the asynchronous machines through magnetic signature analysis using finite-element method and neural networks," *IEEE Trans. Energy Convers.*, vol. 28, no. 4, pp. 1064–1071, Dec. 2013.
[15] M. Barzegaran and O. Mohammed, "Condition monitoring of power components in electric grid using electromagnetic stray fields," *Elect. Eng.*, vol. 100, no. 2, pp. 499–508, Jun. 2018.
[16] A. Lelong, M. O. Carrion, V. Degardin, and M. Lienard, "Characterization of electromagnetic radiation caused by on line wire diagnosis," in *Proc. 29th General Assembly of Int. Union Radio Sci.*, 2008, pp. 1–4.
[17] M. Barzegaran, A. Mohamed, T. Youssef, and O. A. Mohammed, "Electromagnetic signature study of a power converter connected to an electric motor drive," *IEEE Trans. Magn.*, vol. 50, no. 2, pp. 201–204, Feb. 2014.
[18] R. Biswas, A. Routray, S. Sengupta, M. Pramanik, and A. K. Gupta, "EMR signature analysis for health monitoring and early stage fault diagnosis of IGBT," in *Proc. 43rd Annu. Conf. IEEE Ind. Electron. Soc.,* 2017, pp. 5043–5048.
[19] Y.-D. Huang and M. Barkat, "Near-field multiple source localization by passive sensor array," *IEEE Trans. Antennas Propag.*, vol. 39, no. 7, pp. 968–975, Jul. 1991.
[20] M. Diao and S.-L. Miao, "New method of parameter matching for 2-D ESPRIT algorithms," *Syst. Eng. Electron.*, vol. 29, no. 8, pp. 1226–1229, 2007.
[21] F. Wen and W. P. Tay, "Localization for mixed near-field and far-field sources using data supported optimization," in *Proc. 15th Int. Conf. Inf. Fusion*, 2012, pp. 402–407.
[22] A. Dhar, A. Senapati, and J. S. Roy, "Direction of arrival estimation for smart antenna using a combined blind source separation and multiple signal classification algorithm," *Indian J. Sci. Technol.*, vol. 9, no. 18, 2016.
[23] C. R. Paul, *Introduction to Electromagnetic Compatibility*, vol. 184. Hoboken, NJ, USA:Wiley, 2006.
[24] G. L. Skibinski, R. J. Kerkman, and D. Schlegel, ''EMI emissions of modern PWM ac drives," *IEEE Ind. Appl. Mag.*, vol. 5, no. 6, pp. 47–80, Nov./Dec. 1999.
[25] K. Oh, "IGBT basics 1," Fairchild Semiconductor Corporation, Sunnyvale, CA, USA, Appl. Note AN9016, 2001.
[26] K. Sheng, S. J. Finney, and B. W. Williams, "Thermal stability of IGBT high-frequency operation," *IEEE Trans. Ind. Electron.*, vol. 47, no. 1, pp. 9–16, Feb. 2000.
[27] R. F. Pierret and G. W. Neudeck, *Advanced Semiconductor Fundamentals*, vol. 6. Reading, MA, USA: Addison-Wesley, 1987.
[28] S. M. Sze and K. K. Ng, *Physics of Semiconductor Devices*. Hoboken, NJ, USA: Wiley, 2006.
[29] B. S. Guru and H. R. Hiziroglu, *Electromagnetic Field Theory Fundamentals*. Cambridge, U.K.: Cambridge Univ. Press, 2004.
[30] Z. Sarkany, A. Vass-Varnai, and M. Rencz, "Comparison of different power cycling strategies for accelerated lifetime testing of power devices," in *Proc. Electron. System-Integr. Technol. Conf.*, 2014, pp. 1–5.
[31] T. S. Dhope, "Application of music, esprit and root music in DOA estimation," Faculty Elect. Eng. Comput., Univ. Zageb, Croatia, 2010.
[32] L.-Y. Zhang and D.-S. Yang, "DOA estimation based on music algorithm using an array of vector hydrophones," *J. Harbin Eng. Univ.*, vol. 1, 2004, Art. no. 6.

Rajashree Biswas received the B.Tech. degree from Biju Pattnaik University, Rourkela, India, in 2011. She received the master's degree from the National Institute of Technology (NIT) Rourkela, Rourkela, India, in 2013. She is currently working toward the Ph.D. degree at the Department of Electrical Engineering, IIT Kharagpur, Kharagpur, India.

Her research interests include power-electronics monitoring and fault diagnosis, electromagnetic radiation study of power electronics components, and application of signal processing in fault detection and diagnosis.

Aurobinda Routray received the master's degree from the Indian Institute of Technology Kanpur, Kanpur, India, in 1991 and the Ph.D. degree from Sambalpur University, Sambalpur, Odisha, India, in 1999.

He has also worked as a Postdoctoral Researcher at Purdue University, West Lafayette, IN, USA, during 2003–2004. He is currently working as a Professor with the Department of Electrical Engineering, Indian Institute of Technology Kharagpur, Kharagpur India. His research interests include nonlinear and statistical signal processing, signal-based fault detection and diagnosis, real time and embedded signal processing, numerical linear algebra, and data-driven diagnostics.